Controlled synthesis of $CaTiO_3:Ln^{3+}$ nanocrystals for luminescence and photocatalytic hydrogen production

Ling Meng, Kaifu Zhang, Kai Pan, Yang Qu* and Guofeng Wang*

Received (in XXX, XXX) Xth XXXXXXXXX 200X, Accepted Xth XXXXXXXXX 200X
First published on the web Xth XXXXXXXXX 200X
DOI: 10.1039/b000000x

Bifunctional $CaTiO_3:Ln^{3+}$ (Ln = Eu and Er) nanocrystals were prepared via a facile method and followed by calcination in air. The as-prepared $CaTiO_3:Ln^{3+}$ nanocrystals exhibit bifunctional performance in the photoluminescence and photocatalytic hydrogen production. As phosphor powder, the luminescence properties $CaTiO_3:Ln^{3+}$ nanocrystals could be controlled by doping with different Ln^{3+} ions. They showed very stable luminescence properties and a much higher quenching concentration due to the scheelite related structure of $CaTiO_3$, which is up to 17% (Eu doping). As photocatalyst, the $CaTiO_3:Ln^{3+}$ nanocrystals exhibited a higher activity for hydrogen production under ultraviolet light irradiation. The $CaTiO_3:Er^{3+}$ nanocrystals display the highest photocatalytic activity, which is up to 461.25 $\mu mol\cdot h^{-1}$, it is higher than that of $CaTiO_3:Eu^{3+}$ nanocrystals and pure $CaTiO_3$. The results indicated that the incorporation of Ln^{3+} ions benefits the electron transfer as well as the reduction of the band gap of $CaTiO_3$ photocatalyst.

1. Introduction

The special spectroscopic properties of rare-earth (RE) ions in different host lattices are applied to many aspects, including lamp phosphors, radiation monitoring, lasers, and white light-emitting diodes and so on.[1-6] These applications depend strongly on the luminescence properties, which are relative to the morphology and composition of the materials. Although the substantially shielded transitions of RE ions, the luminescent properties of nanocrystals are also affected by RE ion size, shape, crystal structure, and chemical composition of the materials.[7-11] In recent years, the controllable synthesis of nanocrystals has attracted considerable interest due to their significance in basic scientific research and potential technological applications, based on their specific geometries and distinct properties.[12-14] A limited amount of precursor and synthesis process is used to control the growth to achieve nanostructures with clean surfaces, which is required for high-performance electric and optical applications.[15-17]

$CaTiO_3$ is one of the alkaline earth titanates with perovskite structure and interesting electronic, optical, magnetic and catalytic properties, due to its excellent resistance against photocorrosion, high thermal stability and the structure stability when doped with metal ions to alter the opto-electrical properties. RE ion doped $CaTiO_3$ as optical materials have been studied by some researchers because of the well-known high chemical durability and thermal stability of $CaTiO_3$ nanocrystals in this field, for example, high color rendering index, high luminescence efficiency, long life time, low power consumption, and friendly to environment.[18,19]

Moreover, photocatalytic hydrogen production from water using a semiconductor nanomaterial has attracted a tremendous amount of interest.[20-23] Over the past several decades, many photocatalysts have been found to have photocatalytic activities for photocatalytic hydrogen production.[24-27] Thermodynamically, water splitting into H_2 and O_2 is an uphill reaction, accompanied by a large positive change in the Gibbs free energy.[28] Thus, a suitable semiconductor is urgent needed. $CaTiO_3$ is also a wide band gap (~3.5 eV) semiconductor, but its conduction band is very negative (-0.86 eV *vs.* NHE) which is efficient to reduce proton to hydrogen. [29,30] If the band gap is reduced by doping with RE metals, it would be one of the most efficient methods to improve its photocatalytic activity, related to the vacant f orbitals of the rare earth metal ions that allow for intermediate energy states, reducing the band gap thus enhancing the photoactivity.[31]

Based on the consideration above, we report a bifunctional materials of $CaTiO_3:Ln^{3+}$ (Ln = Eu and Er) with excellent luminescence properties and photocatalytic hydrogen production activity. Importantly, the concomitant impurities of $CaCO_3$ was overcame and pure phase $CaTiO_3$ nanocrystals was successfully prepared by sol-gol method. Compared with hydrothermal method, sol-gol method could ensure the combination of Ca and Ti in stoichiometry with out dissociative Ca^{2+} to form $CaCO_3$. Novel luminescence properties and higher activity for photocatalytic hydrogen production were displayed owing to the unique perovskite structure of $CaTiO_3$ and RE ion doping which increased the BET surface areas as well as reduced the band gaps and improved the charge separation, proven by the electrochemical measurement.

2. Experimental section

2.1 Preparation of samples

[a] *Key Laboratory of Functional Inorganic Material Chemistry, Ministry of Education of the People's Republic of China, Heilongjiang University, Harbin 150080 P. R. China; E-mail: copy0124@126.com; wanggf75@gmail.com*
Electronic Supplementary Information (ESI) available: [Table S1, Figure S1-S7]. See DOI: 10.1039/x0xx00000x

Preparation of samples: All of the chemicals used in this paper were analytical-grade and used without further purification. A typical synthesis of $CaTiO_3$ nanocrystals was as follows: 1.58 g calcium acetate ($Ca(CH_3COO)_2 \cdot 2H_2O$) and 3.4 ml tetrabutyl titanate ($Ti(OC_4H_9)_4$) were dissolved in 30 ml ethylene glycol, then the solution was stirred at room temperature for about 30 min. Then, the milky suspensions was dried in air at 180 °C for 24 h and sintered at 600 °C for 2 h. For comparison, the mentioned milky suspensions above was hydrothermal treatment at 180 °C for 24 h and sintered at 600 °C for 2 h.

$CaTiO_3:Ln^{3+}$ (Ln = Eu and Er) nanocrystals were prepared by the same procedure, except for adding additional $Ln(NO_3)_3$ into the solution of ethylene glycol at the initial stage.

2.2 Characterization

Characterization: The crystal structure was analyzed by a Rigaku (Japan) D/MAX-rA X-ray diffractometer (XRD) equipped with graphite monochromatized Cu Kα radiation (γ=1.541874 Å), keeping the operating voltage and current at 40 kV and 40 mA, respectively. The size and morphology of the final products were determined by using JSM-6301F scanning electron microscope (SEM, Tokyo, Japan) and JEM-2010F transmission electron microscope (TEM, JEOL, Tokyo, Japan) operated at 200 kV. Nitrogen adsorption-desorption isotherms were collected using an Autosorb-1 (Quantachrome Instruments, Boynton Beach, FL) nitrogen adsorption apparatus at 77 K. The pore size distribution plots were obtained by the Barrett–Joyner–Halenda (BJH) model. Ultraviolet-visible (UV-vis) absorption spectra were determined by a UV-vis spectrophotometer (Shimadzu UV-2550, Tokyo, Japan).

The photocatalytic H_2 evolution from water was conducted in an online photocatalytic hydrogen production system (AuLight, Beijing, China, CEL-SPH2N). A powder sample of the catalyst (0.1 g) was suspended in a mixture of 80 ml distilled water and 20 ml methanol in the cell by using a magnetic stirrer. Pt-loaded photocatalysts were prepared by known standard method of in situ photo-deposition method. Before the reaction, the mixture was deaerated by evacuation to remove O_2 and CO_2 dissolved in water. The reaction was carried out by irradiating the mixture with UV light from a 300 W Xe lamp with a 320-390 nm reflection filter which means the wavelength of light is approximately 320-390 nm. Gas evolution was observed only under photo-irradiation, being analyzed by an online gas chromatograph (SP7800, thermal conductivity detector, molecular sieve 5 Å, N_2 carrier, Beijing Keruida Limited, Beijing, China).

3. Results and Discussion

3.1 Crystal structures and morphologies

In the preparation of $CaTiO_3$, control the generated impurity of $CaCO_3$ is important. Figure S1a shows the XRD patterns of pure $CaTiO_3$ nanocrystals without doping. No peaks corresponding to any other phases or impurities were detected, indicating the high purity. SEM, TEM and HRTEM (Figure S1b and c) show the particle size is approximately 50 nm. The interplanar spacing of 0.27 nm corresponding to the distance of the {200} planes of the orthorhombic phase $CaTiO_3$ is observed. In addition, XRD patterns of samples prepared at different conditions including the solvent, concentration and reaction manners in Figure S2 indicate that $CaCO_3$ appears in these conditions. This means that $CaTiO_3$ nanoparticles without impurities could be controllable prepared by adjusting the reaction conditions. Figure S3 shows the Mott–Schottky plots of $CaTiO_3$ nanocrystals, of which show positive slopes that implies $CaTiO_3$ is a n-type semiconductors.[32] Flat band potential of the $CaTiO_3$ nanocrystals was found to be -1.5 V (versus Ag/AgCl) indicated that the hydrogen production ability of $CaTiO_3$ is well.

The XRD patterns of $CaTiO_3:Eu^{3+}$ and $CaTiO_3:Er^{3+}$ with different doping concentrations as shown in Figure S4 and S5. It could be observed that after doping with RE ions of Eu and Er, even with different amount, the crystal structure is remained. The morphology of the nanoparticles after doping was studied by TEM and HRTEM which are shown in Figure 1. The high-resolution HRTEM image shows an interplanar spacing of 0.27 nm corresponding to the {200} planes of the ortnorhombic phase $CaTiO_3$, which is not changed as well. In order to study the doping elements, energy-dispersive x-ray (EDX) analysis is taken, as shown in Figure S6. It can be seen that the samples are composed of Ca, Ti, O elements for pure $CaTiO_3$ and Eu and Er for the doping ones, respectively. These results give the evidence that $CaTiO_3:Ln^{3+}$ (Ln = Eu and Er) nanocrystals are prepared. The photophysics properties are also measured to make the bifunctional mechanism clearly. According to the above analysis, Ln^{3+} (Eu and Er) doping pure $CaTiO_3$ nanocrystals were successfully prepared. The RE ions doping didn't change the crystal structure and the crystallinity of pure $CaTiO_3$ nanocrystals.

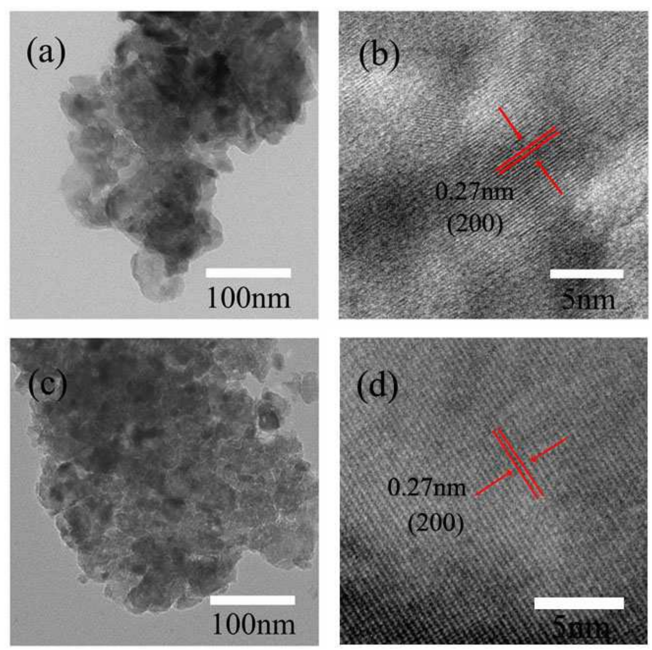

Figure 1. TEM and HRTEM images of (a,b) $CaTiO_3:Eu^{3+}$(0.5%) and (c,d) $CaTiO_3:Er^{3+}$(0.5%) nanocrystals.

3.2 Luminescence spectra of $CaTiO_3$: Eu^{3+} nanocrystals

The doping concentration of RE ion could affect the luminescence property.[33] Generally speaking, the more doping concentration, the better of the luminescence property it is.

However, a contradiction that the more doping may lead to the lattice deformation and further influence the property. Perovskite structure oxides are very stable and the unique feature make them suitable for the substance of phosphor. The emission spectra of the $CaTiO_3:Eu^{3+}$ nanocrystals excited at 397 nm was studied and shown in Figure 2a. Obviously, the spectral configurations of $CaTiO_3:Eu^{3+}$ nanocrystals unchanged with the Eu^{3+} contents. In addition, the maximum Eu^{3+} concentrations is 17% mol% of the $^5D_0 \rightarrow {}^7F_2$ transition. The excitation spectra of the $CaTiO_3:Eu^{3+}$ nanocrystals prepared with different $Eu(NO_3)_3$ contents of the reactant monitored at 619 nm are shown Figure 2b.

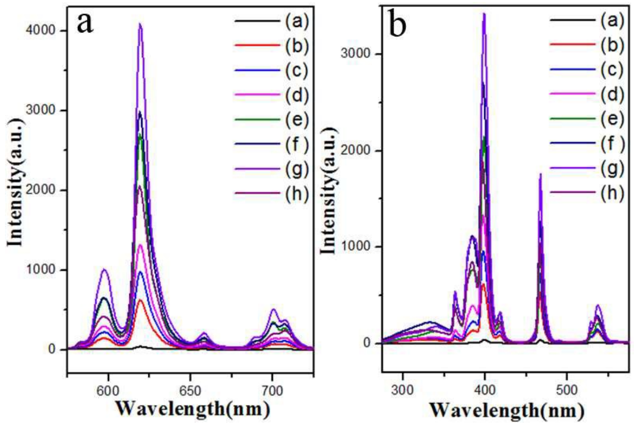

Figure 2. Emission (left, λ_{ex} = 397 nm) and excitation (right, λ_{em} = 619 nm) spectra of (a) $CaTiO_3:Eu^{3+}$(0.5%), (b) $CaTiO_3:Eu^{3+}$(5%), (c) $CaTiO_3:Eu^{3+}$(7%), (d) $CaTiO_3:Eu^{3+}$(10%), (e) $CaTiO_3:Eu^{3+}$(13%), (f) $CaTiO_3:Eu^{3+}$(15%), (g) $CaTiO_3:Eu^{3+}$(17%) and (h) $CaTiO_3:Eu^{3+}$(20%).

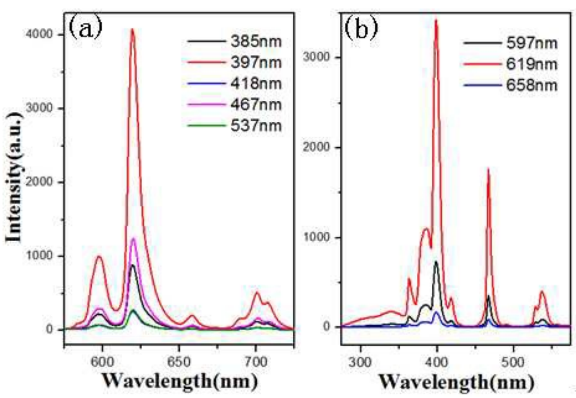

Figure 3. (a) Emission spectra of $CaTiO_3:Eu^{3+}$(17%) nanocrystals excited at different wavelengths. (b) Excitation spectra of $CaTiO_3:Eu^{3+}$(17%) monitored at different emission wavelengths.

Figure 3a shows the emission spectra of the $CaTiO_3:Eu^{3+}$ (17%) nanocrystals excited at different excitation wavelengths. The $^5D_0 \rightarrow {}^7F_1$ (589 ~ 602 nm), $^5D_0 \rightarrow {}^7F_2$ (615 ~ 633 nm), $^5D_0 \rightarrow {}^7F_3$ (~654 nm), and $^5D_0 \rightarrow {}^7F_4$ (~713 nm) transitions of Eu^{3+} were observed. The emission intensity was the strongest when the excitation was performed at 397 nm. Because the 4f energy levels of Eu^{3+} are hardly affected by the crystal field, there is no notable shift in the positions of the emission peaks compared to other Eu^{3+}-doped systems.[36] The $^5D_0 \rightarrow {}^7F_1$ transition is magnetic-dipole-allowed and its intensity is almost independent on the local environment around Eu^{3+} ions. The $^5D_0 \rightarrow {}^7F_2$ transition is electric-dipole-allowed due to an admixture of opposite parity $4f^{n-1}5d$ states by an odd parity crystal-field component. Therefore, its intensity is sensitive to the local structure around Eu^{3+} ions. The $^5D_0 \rightarrow {}^7F_3$ transition exhibits a mixed magnetic dipole and electric dipole character. The $^5D_0 \rightarrow {}^7F_4$ is an electric dipole transition. The $^5D_0 \rightarrow {}^7F_1$ is dominating in a site with inversion symmetry, while the $^5D_0 \rightarrow {}^7F_2$ is the strongest in a site without inversion symmetry. Figure 3b shows the excitation spectra of the $CaTiO_3:Eu^{3+}$(17%) nanocrystals monitored at 597, 619 and 658 nm. The positions of the excitation peaks are practically identical to the characteristic absorption bands for f–f intra-configuration transitions in trivalent europium.[14]

3.3 Luminescence spectra of $CaTiO_3:Er^{3+}$nanocrystals

Figure 4 shows the upconversion (UC) luminescence spectra of $CaTiO_3$ nanocrystals with different Er^{3+} concentrations. The spectral peaks correspond to the following transitions: $^2H_{11/2} \rightarrow {}^4I_{15/2}$ (∼526 nm), $^4S_{3/2} \rightarrow {}^4I_{15/2}$ (∼544 nm) and $^4F_{9/2} \rightarrow {}^4I_{15/2}$ (∼662 nm). It was observed that the dominant emissions are located at green luminescence range for the $CaTiO_3:Er^{3+}$ nanocrystals. The relative intensity of $^4F_{9/2} \rightarrow {}^4I_{15/2}$ to $^2H_{11/2}/{}^4S_{3/2} \rightarrow {}^4I_{15/2}$ rises with increasing the Er^{3+} content. When Er^{3+} concentration is 10%, the luminescence was almost vanished due to luminescence quenching. The CIE coordinates of the UC luminescence were (0.309, 0.511), (0.313, 0.496) and (0.318, 0.45) for the $CaTiO_3:Er^{3+}$(0.5%), $CaTiO_3:Er^{3+}$(3%) and $CaTiO_3:Er^{3+}$(5%), respectively. Obviously, the CIE coordinates changed with the different Er^{3+} concentrations.

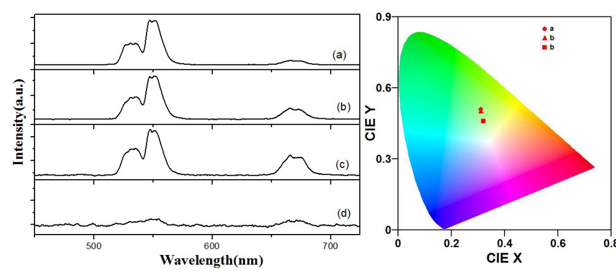

Figure 4. UC luminescence spectra and corresponding CIE 1931 chromaticity diagram of (a) $CaTiO_3:Er^{3+}$(0.5%), (b) $CaTiO_3:Er^{3+}$(3%), (c) $CaTiO_3:Er^{3+}$(5%) and (d) $CaTiO_3:Er^{3+}$(10%) nanocrystals.

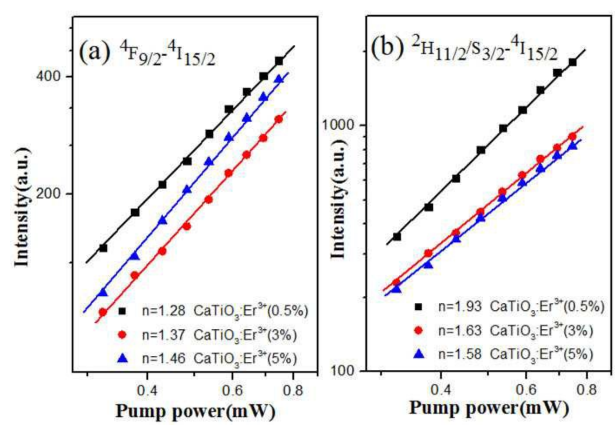

Figure 5. Dependence of the UC emission intensities on the excitation power in the $CaTiO_3$ nanocrystals with different Er^{3+} concentrations nanocrystals.

Dependence of the UC luminescence intensity on pump power was actually performed to obtain a better understanding of the UC processes. For an unsaturated UC process, the emission intensity (I_f) will be proportional to some power (n) of the infrared excitation (P) power: $I_f \& P^n$, where n is the number of infrared photons absorbed per visible photon emitted. Figure 5 shows the double logarithmic plots of the emission intensity as a function of excitation power for the $^4S_{3/2}/^2H_{11/2} \rightarrow {}^4I_{15/2}$ and $^4F_{9/2} \rightarrow {}^4I_{15/2}$ emissions. For the red mission, the values of n were separately determined to be 1.26, 1.37 and 1.46 for the $CaTiO_3:Er^{3+}$(0.5%), $CaTiO_3:Er^{3+}$(3%) and $CaTiO_3:Er^{3+}$(5%), suggesting that a two-photon process should be involved for populating the red levels. For the green transitions, the values of n were separately determined to be 1.95, 1.63 and 1.58 for the $CaTiO_3:Er^{3+}$(0.5%), $CaTiO_3:Er^{3+}$(3%) and $CaTiO_3:Er^{3+}$(5%), suggesting that a two-photon process should be involved for populating the green levels.

3.4 Photocatalytic activity of $CaTiO_3:Ln^{3+}$nanocrystals

Metal ions doping wide band gap semiconductor is an effective strategy to improve the light absorption and charge separation, that further improve the photocatalytic performance.[34-35] Although the conduction band of $CaTiO_3$ is much negative to reduce proton, the band gap of it is so wide which is unfavourable to the light absorption. The prepared $CaTiO_3:Ln^{3+}$ (Ln = Eu and Er) nanocrystals is thus believed to be excellent catalysts for photocatalytic hydrogen production. According to the luminescence property, $CaTiO_3:Er^{3+}$(0.5%) and $CaTiO_3:Eu^{3+}$(0.5%) nanocrystals is utilized as photocatalysts for hydrogen production. The optical absorptions of the samples were conducted with a UV-vis absorption spectrometer, as shown in Figure 6. All the samples show the absorption band edge at in the UV light region (λ<400 nm), implies these are wide band semiconductors. The band gap (Eg) of the $CaTiO_3:Er^{3+}$(0.5%) and $CaTiO_3:Eu^{3+}$(0.5%) are calculated to be about 3.3 eV from the onset of the absorption edge (inset of Figure 6). However, compare to $CaTiO_3:Eu^{3+}$(0.5%), $CaTiO_3:Er^{3+}$(0.5%) show a little enhanced light absorption from 400 to 700 nm as shown in Figure 6. This interesting phenomenon may be attributed to the special molecular orbital structure of Er. In addition, the absorption peaks of $CaTiO_3:Er^{3+}$ correspond to the f-f transitions of Er^{3+} ions: $^4I_{15/2} \rightarrow {}^2H_{11/2}$, $^4I_{15/2} \rightarrow {}^4S_{3/2}$ and $^4I_{15/2} \rightarrow {}^4F_{9/2}$.[36]

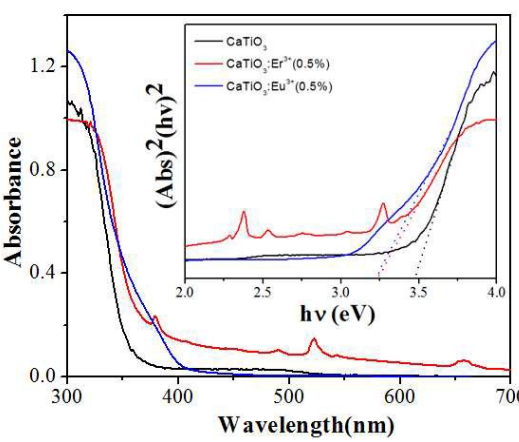

Figure 6. UV–vis absorption spectra of $CaTiO_3$, $CaTiO_3:Er^{3+}$(0.5%) and $CaTiO_3:Eu^{3+}$(0.5%) nanocrystals.

Figure 7 shows that the time depended H_2 evolution over the samples under UV light irradiation. Obviously, the photocatalytic performance of $CaTiO_3:Er^{3+}$(0.5%) is better than $CaTiO_3$ and $CaTiO_3:Eu^{3+}$(0.5%) nanocrystals. The average H_2 production yield is up to 461.25 μmol·h^{-1}. This is in accordance with the light absorption that may improve the generation of photo-electron that promote the photocatalytic activity. Except that, the surface area is significant to photocatalytic activity because it would produce more reaction site and improve the surface catalysis to produce hydrogen.

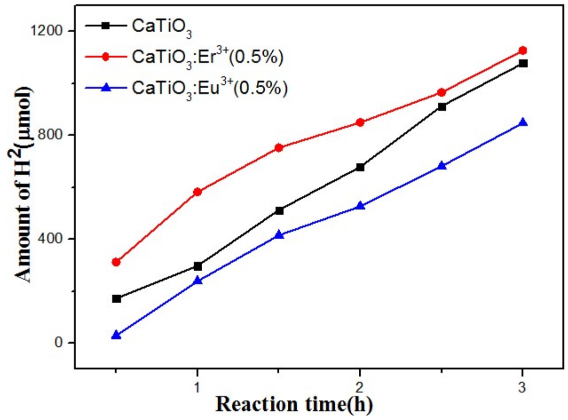

Figure 7. H_2 production activity of the $CaTiO_3$, $CaTiO_3:Er^{3+}$(0.5%) and $CaTiO_3:Eu^{3+}$(0.5%) nanocrystals under UV light irradiation.

The N_2 adsorption–desorption isotherms and the corresponding BJH pore size distribution plots of the samples (Figure S7) shows that the Brunauer-Emmett-Teller (BET) surface areas of the pure $CaTiO_3$, $CaTiO_3:Er^{3+}$(0.5%) and $CaTiO_3:Eu^{3+}$(0.5%) nanocrystals are 18.48, 19.58 and 17.57 m^2/g, respectively. Obviously, the BET surface areas of $CaTiO_3:Er^{3+}$ nanocrystals are larger that of pure $CaTiO_3$ and $CaTiO_3:Er^{3+}$ nanocrystals on account of the radius of Er^{3+} ions are smaller than that of Ca^{2+} and Eu^{3+} ions, which is very advantageous for photocatalytic hydrogen production, this demonstrates that the surface area play important role in this work.

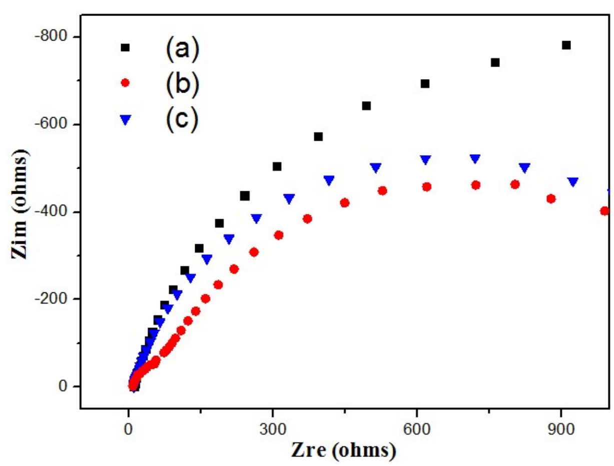

Figure 8. EIS Nynquist plots of (a) $CaTiO_3$ and (b) $CaTiO_3:Er^{3+}$(0.5%), (c) $CaTiO_3:Er^{3+}$(0.5%) nanocrystals. (scanning the frequency from 1 MHz to 0.5 Hz at a bias of 0.5 V under UV light irradiation)

The photoelectrochemical measurement could reflect the charge transport of semiconductors.[37,38] Figure 8 shows the typical EIS Nyquist plots of the samples under UV light irradiation. While the measurements show a bit smaller interfacial resistance for the $CaTiO_3:Er^{3+}$(0.5%) than that of $CaTiO_3$ under UV light irradiation, indicating a more efficient charge separation and fast electron transport. The photoelectrochemical result show that the Er doping is acceptable for $CaTiO_3$ as photocatalys for hydrogen production. Although the mechanism deep inside is not clear, such as what kind of special molecular orbital affect the light absorption and the orbital interaction between Er and $CaTiO_3$, it is sure that the rare-earth ions doping is beneficial to the photocatalytic hydrogen production.

4. Conclusions

Bifunctional $CaTiO_3:Ln^{3+}$ (Ln = Eu and Er) nanocrystals without any impurities was facile prepared. The usually accompanying impurity $CaCO_3$ was overcame by using ethylene glycol as stabilizer. The $CaTiO_3:Ln^{3+}$ (Ln = Eu and Er) nanocrystals exhibited both luminescence properties and photocatalytic hydrogen production activities. The luminescence results indicated pure $CaTiO_3$ promoted the RE luminescence properties and increased the quenching concentration, which is up to 17%. At the same time, doped the RE ions improved light absorption as well as increased BET surface areas to enhance the photocatalytic hydrogen production activity, and $CaTiO_3:Er^{3+}$ (0.5%) displayed the optimal activity which could be explained by photoelectrochemical which indicating a more efficient charge separation. This novel and high effective bifunctional material is believed to have potential application in the fields of photochemistry and photophysics.

Acknowledgments

This work was supported by the National Natural Science Foundation of China (21171052, 21471050, 21501052 and 21473051), the China Postdoctoral Science Foundation (2015M570304), Program for Innovative Research Team in University (IRT-1237), Heilongjiang Province Natural Science Foundation (ZD201301, QC2015010).

References

1 S. L. Gai, C. X. Li, P. P. Yang and J. Lin, Chem. Rev., 2014, 114, 2343-2389.
2 Y. H. Yuan, R. S. Li, Q. Wang, Z. L. Wu, J. Wang, H. Liu and C. Z. Huang, Nanoscale., 2015, 7, 16841-16847.
3 J. Zhou, Z. Liu and F. Y. Li, Chem. Soc. Rev., 2012, 41, 1323-1349.
4 C. Feldmann, T. Jüstel, C. R. Ronda and P. J. Schmidt, Adv. Funct. Mater., 2003, 13, 511-516.
5 Z. Gu, L. Yan, G. Tian, S. Li, Z. Chai and Y. Zhao, Adv. Mater., 2013, 25, 3758-3779.
6 Z. Chen, W. Zheng, P. Huang, D. T. Tu, S. Y. Zhou, M. D. Huang and X. Y. Chen, Nanoscale., 2015, 7, 4274-4290.
7 T. Y. Sun, D. Q. Zhang, X. F. Yu, Y. Xiang, M. Luo, J. H. Wang, G. L. Tan, Q. Q. Wang and P. K. Chu, Nanoscale., 2013, 5, 1629-1637.
8 C. M. Zhang, J. Lin,Chem. Soc. Rev., 2012, 41, 7938-7961.
9 L. Song, X. Y. Zhao, L. X. Cao, J. W. Moon, B. H. Gu and W. Wang, Nanoscale., 2015, 7, 16695-16703.
10 Y. B. Dong, P. Wang, J. P. Ma, X. X. Zhao, H. Y. Wang, B. Tang and R. Q. Huang, J. Am. Chem. Soc., 2007, 129, 4872.
11 L. Gan, F. F. Xu, X. H. Zeng, Z. S. Li, Z. Y. Mao, P. Lu, Y. C. Zhu, X. J. Liu and L. L. Zhan, Nanoscale., 2015,7, 11393-11400.
12 D. M. Yang, X. J. Kang, M. M. Shang, G. G. Li, C. Peng, C. X. Li and J. Lin, Nanoscale., 2011, 3, 2589-2595.
13 S. L. Gai, C. X. Li, P. P. Yang, J. Lin, Chem. Rev., 2014, 114, 2343-2389.
14 G. F. Wang, Q. Peng and Y. D. Li, Acc. Chem. Res., 2011, 44, 322-332.
15 H. G. Cha, K. S. Choi, Nature. Chem., 2015. 7. 328-333.
16 H. Kim, J. Park, I. Park, K. Jin, S. E. Jerng, S. H. Kim, K. T. Nam and K. Kang, Nat. Commun., 2015, 6, 8253.
17 J. Park, W. Lee, T. Choi, S. H. Hwang, J. M. Myoung, J. H. Jung, S. H. Kim and H. Kim, Nanoscale., 2015, 7, 1308-1313.
18 M. H. Song, J. C. Yu, D. B. Kim, E. D. Jung and B. R. Lee, Nanoscale., 2015, 00, 1-3.
19 X. F. Yang, J. X. Fu, C. J. Jin, J. Chen, C. L. Liang, M. M. Wu and W. Z. Zhou, J. Am. Chem. Soc., 2010, 132(40), 14279-14287.
20 A. Fujishima and K. Honda, Nature., 1972, 238, 37-38.
21 H. Y. Li, H. W. Yu, L. Sun, J. L. Zhai and X. R. Han, Nanoscale., 2015, 7, 1610-1615.
22 H. Tong, S. X. Ouyang, Y. P. Bi, N. Umezawa, M. Oshikiri and J. H. Ye, Adv. Mater., 2012, 24, 229-251.
23 A. Kubacka, M. F. García and G. Colón, Chem. Rev., 2012, 112(3), 1555-1614.
24 X. Chen, S. Shen, L. Guo, and S. S. Mao, Chem. Rev., 2010, 110(11), 6503-70.
25 Q. Li, B. Guo, J. Yu, J. Ran, B. Zhang, H. Yan, and J. R. Gong, J. Am. Chem. Soc., 2011, 133(28), 10878-84.
26 A. P. Bhirud, S. D. Sathaye, R. P. Waichal, J. D. Ambekar, C. J. Park and B. B. Kale, Nanoscale., 2015, 7, 5023-5034.
27 T. Yang, X. W. Chang, J. H. Chen, K. C. Chou and X. M. Hou, Nanoscale., 2015,7, 8955-8961.
28 A. Linsebigler, G. Lu, and J. Yates, Chem. Rev., 1995, 95, 735.
29 A. Garcia and J. E. Northrup, Phys. Rev. Lett., 1995, 74, 1131–1134.
30 K. Ueda, H. Yanagi, R. Noshiro, H. Hosono and H. Kawazoe, J. Phys. Condens. Matter., 1998, 10, 3669–3677.
31 J. Chen, S. H. Shen, P. Wua and L. J. Guo, Green Chem., 2015, 17, 509-517.
32 Y. Qu, W. Zhou, Z. Y. Ren, C. G. Tian, J. L. Li, H. G. Fu, ChemPlusChem., 2014, 79(7), 995-1000.
33 G. F. Wang, Y. Li, B. J. Jiang, K. Pan, N. Y. Fan, Q. M. Feng, Y. J. Chen, C. G. Tian, Chem. Commun., 2011, 47, 8019-8021.
34 J. Zhou, Q. Liu, W. Feng, Y. Sun, F. Y. Li, Chem. Rev., 2015, 115, 395-465.
35 H. Terraschke, C. Wickleder, Chem. Rev., 2015, 115, 11352-11378.
36 J. Tang, L. Chen, J. Li, Z. Wang, J. H. Zhang, L. G. Zhang, Y. S. Luo and X. J. Wang, Nanoscale., 2015, 7, 14752-14759.
37 H. J. Li, Y. Zhou, W. G. Tu, J. H. Ye, Z. G. Zou, Adv. Funct. Mater., 2015, 25, 998-1013.
38 D. Friebel, M. W. Louie, M. Bajdich, K. E. Sanwald, Y. Cai, A. M. Wise, M. J. Cheng, D. Sokaras, T. C. Weng, R. Alonso-Mori, J. Am. Chem. Soc., 2015, 137, 1305-1313.

Controlled synthesis of $CaTiO_3$:Ln^{3+} nanocrystals for luminescence and photocatalytic hydrogen production

Ling Meng, Kaifu Zhang, Kai Pan, Yang Qu* and Guofeng Wang*

Key Laboratory of Functional Inorganic Material Chemistry, Ministry ofEducation, School of Chemistry and Materials Science, Heilongjiang University, Harbin, 150080, P. R. China.

E-mail: copy0124@126.com;wanggf_w@163.com

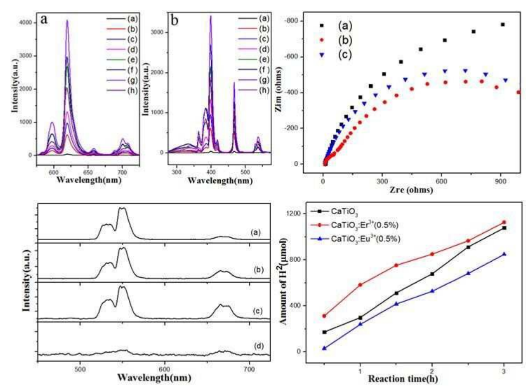

Bifunctional $CaTiO_3$:Ln^{3+} (Ln = Eu and Er) nanocrystals were prepared via a facile method and followed by calcination in air. The as-prepared $CaTiO_3$:Ln^{3+} nanocrystals not only can show very stable luminescence properties and a much higher quenching concentration due to the scheelite related structure of $CaTiO_3$, but also can exhibit a higher activity for hydrogen production under ultraviolet light irradiation. The $CaTiO_3$:Er^{3+} nanocrystals display the highest photocatalytic activity, which is up to 461.25 $\mu mol \cdot h^{-1}$, it is higher than that of $CaTiO_3$:Eu^{3+} nanocrystals and pure $CaTiO_3$.